Analytical and numerical study of subradiance-only collective decay from atomic ensembles

Anirudh Yadav and D. D. Yavuz
Department of Physics, 1150 University Avenue, University of Wisconsin–Madison, Madison, Wisconsin 53706, USA

(Received 15 March 2024; revised 13 June 2024; accepted 8 July 2024; published 5 August 2024)

We analytically and numerically study collective emission from an ensemble of atoms in the weak-excitation regime with the initial condition of uniform excitation of the ensemble. We show that under certain conditions, subradiance at the later stages of the collective decay does not necessarily need to be accompanied by early-time superradiance. We analyze the conditions where such subradiance-only decay occurs for ordered and disordered ensembles in one-, two-, and three-dimensional spatial configurations.

DOI: 10.1103/PhysRevA.110.023709

I. INTRODUCTION

Since the seminal paper by Dicke [1], collective decay (superradiant or subradiant) of an ensemble of radiators has been studied by many authors, and this problem continues to be relevant for a wide range of physical systems [2–13]. Collective decay has traditionally been studied in ensembles in which there are many atoms within a cubic wavelength of volume. In this limit, which is typically referred to as the Dicke limit, it is relatively straightforward to observe superradiance [1,2]. In this regime, when most of the atoms are excited to a higher energy level, the ensemble primarily decays through in-phase superpositions due to the symmetries in the system (hence resulting in superradiance). Early studies of superradiance were performed many decades ago, primarily in hot atomic vapors [14,15]. Recently, these studies were extended to a variety of different physical systems, including neutral atoms [16–19], ions [20], molecules [21], nitrogen vacancy centers in diamond [22,23], and superconducting Josephson junctions [24].

While most early studies focused on superradiance in the Dicke limit, much recent work has investigated subradiance near or outside the Dicke limit, in particular, using ultracold atomic ensembles [25–32]. Much recent work has shown that even in the dilute regime (i.e., very few atoms per cubic wavelength of volume), the problem is also very rich. Most recently, we demonstrated that collective decay is even relevant in dilute clouds with a very low optical depth [33,34]. Specifically, we demonstrated that the decay rates can be reduced due to subradiance by as much as 20%, with a dilute cloud at an optical depth of 10^{-2} or less. In this regime, subradiant states that are correlated across the whole ensemble are the dominant decay mechanism, as evidenced by the spatial coherence of the emitted light. Specifically, by coupling the emitted light to a Michelson interferometer, we studied the spatial coherence of the light and the dependence of the spatial correlations on the number of atoms and the atomic temperature [34].

The fact that these effects can be observed in disordered and dilute ensembles is not obvious. It is generally believed that early-time superradiance and later-time subradiance go hand in hand [25]. Qualitatively, the physical picture is that, even in a disordered sample, after the initial excitation pulse is switched off, some atoms are at or near the correct positions for their emissions to interfere constructively. These in-phase superpositions cause initial superradiance from the ensemble. The superradiant modes decay out relatively quickly, leaving antiphased superpositions behind, causing subradiance at later times of the temporal evolution. This qualitative picture was also confirmed by numerical simulations by many different authors, showing initial early superradiance (faster than independent decay), followed by subradiance at later times (slower than independent decay).

In this paper, we show that while this qualitative viewpoint is correct for some parameter regime, in general, it is not necessarily an accurate picture. Specifically, we show analytically and numerically that, under certain parameters, subradiance does not necessarily need to be accompanied by early-time superradiance. We take the initial condition for the ensemble to be uniform excitation and focus our attention on the single-atom excited subspace (i.e., weak-excitation regime). We show that under these conditions the ensemble can immediately start to decay with a rate which is slower than the independent decay rate. We refer to this as "subradiance-only" collective decay, and we identify the parameter regimes in one, two, and three dimensions where such decay can happen.

We note that in atomic ensembles, in general, for any parameter regime, one would find collective modes, some of which are superradiant, while others are subradiant. In this paper under uniform excitation of the ensemble (i.e., with the initial condition that the system starts in a state in which each atom has an equal probability of being in the excited state), under certain conditions this initial state has only a projection to the subradiant collective modes. As a result, the decay is subradiant only, in the sense that the ensemble immediately starts to decay with a rate slower than the independent rate.

Before proceeding further, we cite other pertinent prior work. In recent years, interest in collective spontaneous emission, in particular within the context of quantum information science, has increased. Some recent highlights of theory work include highly directional mapping of quantum information between atoms and light in two-dimensional arrays [35,36], studies of broadening and photon-induced atom recoil in collective emission [37–39], light storage in optical lattices [40–42], collective nonclassical light emission and

hyperradiance [11,43,44], and improving photon storage fidelities using subradiance [45]. As we will describe below, our analysis largely relies on an atomic-only exchange Hamiltonian, which is obtained by tracing out the radiation coordinates. This Hamiltonian considers the interaction of N two-level atoms and was used by other authors to study the physics of collective decay. For example, Asenjo-Garcia and colleagues used a similar model to discuss improvements in the subradiant lifetimes in ordered atomic arrays [45]. Robicheaux and Suresh used this simplified two-level approach to develop the mean-field theory of light interacting with atomic arrays [5]. Jenkins and Ruostekoski discussed controlled manipulation of atoms in an atomic lattice using, again, the simplified two-level approach [7].

On the experimental front, as we mentioned above, much early work on subradiance used disordered ultracold atomic clouds [25–32], including our recent work, which used dilute ensembles with low optical depth [33,34]. Recent experiments using ultracold atoms demonstrated single-atomic-layer mirrors [16], phase transitions [46], and enhanced collective coupling using optical cavities [47].

II. EXCHANGE HAMILTONIAN: THE SCHRÖDINGER FORMALISM

When an atomic ensemble undergoes collective decay, one way to model the dipole correlations that build up across the sample is through the reduced atomic-only exchange Hamiltonian. The exchange Hamiltonian has been used to study the physics of collective decay by many different authors. A detailed derivation of this Hamiltonian was discussed in detail, for example, in Ref. [48].

The full Hamiltonian of the whole system consisting of N two-level atoms interacting with a continuum of radiation modes is given by ($\hbar = 1$)

$$\hat{H} = \sum_{j=1}^{N} \frac{\omega_a \hat{\sigma}_j^z}{2} + \sum_{\vec{k},\vec{\epsilon}} \omega_{\vec{k},\vec{\epsilon}} \left(\hat{a}_{\vec{k},\vec{\epsilon}}^{\dagger} \hat{a}_{\vec{k},\vec{\epsilon}} + \frac{1}{2} \right) - \sum_{j=1}^{N} \sum_{\vec{k},\vec{\epsilon}} (g_{\vec{k},\vec{\epsilon}}^{*} \, e^{\vec{k}\cdot\vec{r}_j} \hat{\sigma}_j^{+} \hat{a}_{\vec{k},\vec{\epsilon}} + g_{\vec{k},\vec{\epsilon}} \, e^{-\vec{k}\cdot\vec{r}_j} \hat{\sigma}_j^{-} \hat{a}_{\vec{k},\vec{\epsilon}}^{\dagger}), \quad (1)$$

where

$$\hat{\sigma}_j^{+} = |1_j\rangle\langle 0_j|, \quad \hat{\sigma}_j^{-} = |0_j\rangle\langle 1_j|, \quad (2)$$

$$\hat{\sigma}_j^{z} = |1_j\rangle\langle 1_j| - |0_j\rangle\langle 0_j| \quad (3)$$

are the atomic spin operators for the jth atom with energy eigenstates $|0_j\rangle$ and $|1_j\rangle$, respectively. The quantity ω_a is the atomic transition frequency. The operators $\hat{a}_{\vec{k},\vec{\epsilon}}$ and $\hat{a}_{\vec{k},\vec{\epsilon}}^{\dagger}$, are the photon annihilation and creation operators for a radiation mode with wave vector $\vec{k}$ and polarization $\vec{\epsilon}$.

The well-known Dicke limit can be obtained from the above Hamiltonian when the size of the sample is small compared to the radiation-field length set by the relevant k, i.e., $\vec{k}\cdot\vec{r}_j \to 0 \; \forall \; 0 \leqslant j \leqslant N$. Using the Born-Markov approximation and tracing out the radiation-field part, we can reduce the above full Hamiltonian to the following reduced atomic-only exchange Hamiltonian [48]:

$$\hat{H}_a = \sum_{j=1}^{N} \sum_{\ell=1}^{N} (H_{j\ell} \hat{\sigma}_j^{+} \hat{\sigma}_\ell^{-} + H_{\ell j} \hat{\sigma}_j^{-} \hat{\sigma}_\ell^{+}),$$

where

$$H_{j\ell} = \begin{cases} -i\Gamma/2, & j = \ell, \\ -3i\Gamma[\mathcal{J}(k_a r_{j\ell}) + \cos^2\theta_{j\ell} \mathcal{K}(k_a r_{j\ell})]/4, & j \neq \ell, \end{cases} \quad (4)$$

$$\mathcal{J}(k_a r_{j\ell}) = j_0(k_a r_{j\ell}) - j_1(k_a r_{j\ell})/(k_a r_{j\ell}), \quad (5)$$

$$\mathcal{K}(k_a r_{j\ell}) = 3 j_1(k_a r_{j\ell})/(k_a r_{j\ell}) - j_0(k_a r_{j\ell}), \quad (6)$$

$$r_{j\ell} = \|\vec{r}_j - \vec{r}_\ell\|, \quad \cos\theta_{j\ell} = \frac{\vec{\epsilon}_a \cdot (\vec{r}_j - \vec{r}_\ell)}{r_{j\ell}}. \quad (7)$$

Here, $j_0(z)$ and $j_1(z)$ are spherical Bessel functions, $\vec{\epsilon}_a$ is the direction of the atomic dipoles, and $r_{j\ell}$ is the distance between two specific atoms, atom j and atom ℓ. With the radiation coordinates traced out, each component of the exchange Hamiltonian above describes the process where atom j gets deexcited while emitting a photon, which then gets absorbed by atom ℓ. The quantity $H_{j\ell}$ describes the strength of this exchange interaction between the two atoms.

Using the exchange Hamiltonian above, we can analyze the evolution of the atomic system in the Schrodinger picture. For this purpose, it is convenient to use the basis states of $|q\rangle, q \in \mathbb{B}^N$, which is a binary string for a particular arrangement. We can then describe the evolution of the atomic ensemble using propagation under the exchange Hamiltonian:

$$|\phi(t)\rangle = \sum_{q=0}^{2^N-1} \phi_q(0) e^{-i\hat{H}_a t} |q\rangle = \sum_{q'=0}^{2^N-1} \phi_{q'}(t) |q'\rangle. \quad (8)$$

There are various possible arrangements of the atomic ensemble; the four cases that we study in this paper are shown in the Fig. 1. Specifically, we will consider one-dimensional (1D) and two-dimensional (2D) ordered atomic arrays, as well as 2D and three-dimensional (3D) disordered ensembles of atoms.

III. ANALYTICAL STUDY OF INITIAL-TIME SUPERRADIANCE

Condition for no superradiance

To analytically study early-time behavior of collective decay we define the function $\Phi(t) = \ln\sqrt{\langle\phi(t)\rangle}$, which is the logarithm of the norm of the wave function as a function of time (which is also proportional to the fluorescence of the sample in log scale). We focus on the time derivative of this function, which gives the instantaneous collective decay rate. We can express this time derivative in the following manner:

$$\Phi'(t) = \frac{d}{dt}\frac{1}{2}\ln\langle\phi(t)\rangle = \frac{\mathrm{Re}\left[\langle\phi(t)| \, \frac{d}{dt} |\phi(t)\rangle\right]}{\|\phi(t)\|^2} \quad (9)$$

$$= \frac{\mathrm{Re}[\langle\phi(t)| \, (-i\hat{H}_a) \, |\phi(t)\rangle]}{\|\phi(t)\|^2} = \frac{\mathrm{Im}\langle\hat{H}_a\rangle_t}{\|\phi(t)\|^2}. \quad (10)$$

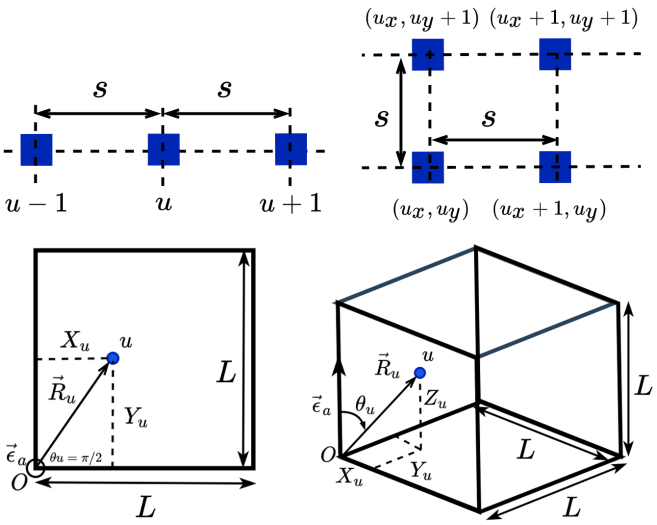

FIG. 1. Four spatial configurations for the atomic sample that we consider in this paper. The plots on the top left and right show ordered one-dimensional and two-dimensional arrays with fixed spacing s between the atoms. The plots on the bottom left and right show disordered two-dimensional and three-dimensional ensembles; the locations of the atoms are uniform random variables along each axis (see text for details).

In the basis of the states $|q\rangle$, $q \in \mathbb{B}^N$, Eq. (10) can be rewritten as

$$\Phi'(t) = \mathrm{Im}\frac{\sum_{q,p}\langle q|\hat{H}_a|p\rangle\,\phi_q^*(t)\phi_p(t)}{\sum_q|\phi_q(t)|^2}. \tag{11}$$

We now restrict the subsequent discussion to the subspace where only a single atom is excited, i.e., $|q\rangle, q \in S = \{0\cdots001; 0\cdots010; 0\cdots100; \cdots\}$. This assumption is essential since it reduces the dimension of the Hilbert space where the evolution is confined from 2^N to N. This subspace can experimentally be accessed by using weak excitation of the ensemble where the Rabi frequency of the excitation pulse is small compared to the decay rate of the excited level. In this subspace we can relabel the basis states by the index of the atom that is excited, $|u\rangle, u = 1 + \log_2 q, q \in S$. In the subspace S with the aforementioned relabeling, the reduced atomic-only exchange Hamiltonian $\hat{H}_a$ has the following matrix-element representation:

$$\langle u|\hat{H}_a|v\rangle = \sum_{j,\ell}(H_{j\ell}\delta_{uj}\delta_{v\ell} + H_{\ell j}\delta_{u\ell}\delta_{vj}) = H_{uv}, \tag{12}$$

$$\langle v|\hat{H}_a|u\rangle = \sum_{j,\ell}(H_{j\ell}\delta_{vj}\delta_{u\ell} + H_{\ell j}\delta_{v\ell}\delta_{uj}) = H_{vu}. \tag{13}$$

Using the above representation, we can rewrite Eq. (11) as

$$\Phi'(t) = \mathrm{Im}\frac{\sum_{u=1,v=1}^{N,N} H_{uv}\phi_u^*(t)\phi_v(t)}{\sum_{u=1}^{N}|\phi_u(t)|^2}. \tag{14}$$

The above expression can be used to evaluate the time derivative (the rate of change) of the total norm of the wave function. We now assume the experimentally relevant case in which we initially have uniform excitation of the ensemble; i.e., at $t = 0$ we have the initial condition $\phi_u(0) = 1/\sqrt{N}$. For this specific

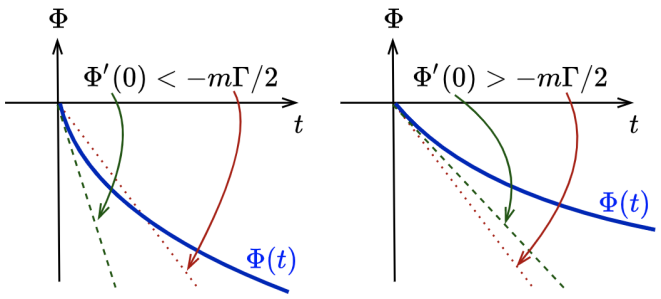

FIG. 2. A visual cartoon schematic for the condition of observing subradiance-only decay. The solid blue line in both plots is the time evolution of $\Phi(t)$. The dashed green line (again in both plots) is the time derivative $\Phi'(0)$, whose slope is the initial collective decay rate, while the dotted red line is the uncorrelated rate. The plot on the left shows the case where $\Phi'(0)$ is lower than the uncorrelated decay rate of $-m\Gamma/2$, hence showing early-time superradiance. The plot on the right shows subradiance-only decay since the initial tangent $\Phi'(0)$ is greater than $-m\Gamma/2$.

initial condition, the initial decay rate of the ensemble is

$$\Phi'(0) = \mathrm{Im}\sum_{u,v} H_{uv}/N. \tag{15}$$

We note that this quantity can be thought of as the initial decay rate of the ensemble since it is the time derivative of the norm of the wave function evaluated at $t = 0$. The condition that we never observe any superradiance can be understood visually, as shown in Fig. 2. When the rate of decay of the atomic sample is slower than the usual uncorrelated ensemble decay rate of $m\Gamma/2$, where m is the number of excited atoms at $t = 0$, then we never observe superradiance. We refer to this as subradiance-only decay. In the subspace of S where $m = 1$, we can express this condition as

$$-\Phi'(0) \leqslant \frac{\Gamma}{2}. \tag{16}$$

Using Eq. (15), we finally obtain

$$-\frac{\Gamma}{2} + \mathrm{Im}\sum_{u,v,u\neq v} H_{uv}/N \geqslant -\frac{\Gamma}{2} \equiv \frac{2}{\Gamma}\mathrm{Im}\sum_{u,v,u\neq v} H_{uv} \geqslant 0. \tag{17}$$

Equation (17) is the central analytical result of this work. Based on Eq. (17), we can now analytically study the conditions under which subradiance-only decay occurs for the four spatial arrangements of atoms shown in Fig. 1.

One-dimensional ordered array of atoms. For the case of a 1D array of atoms in a line at equal spacing of length s with the atomic dipole vector $\vec{\epsilon}_a$ perpendicular to the line, the condition for no superradiance follows from Eqs. (4) and (17),

$$-\frac{3}{2}\sum_{u,v,u\neq v}\mathcal{J}[2\pi(s/\lambda_a)|u-v|] \geqslant 0$$

$$\equiv \left\{I_1'(s/\lambda_a) = \sum_{u=1}^{N-1} 2(N-u)\mathcal{J}[2\pi(s/\lambda_a)u]\right\} \leqslant 0, \tag{18}$$

where the expression I_1' was obtained by summing over all the upper diagonals in the matrix (u, v) except the main diagonal in the sum of Eq. (18). When the number of atoms is very

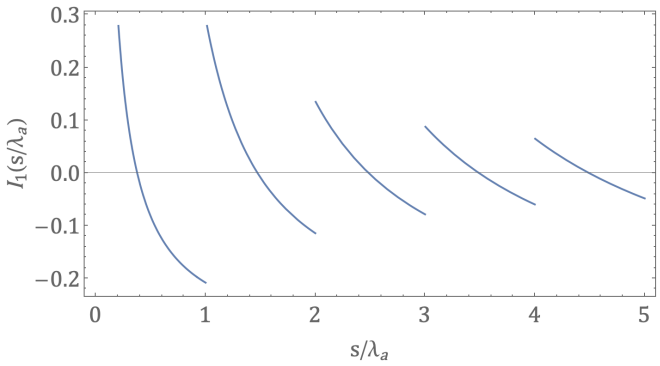

FIG. 3. Plot of I_1 vs s/λ_a. In the regions where $I_1(s/\lambda_a)$ is negative, the condition of Eq. (17) is satisfied, and the decay is subradiance only. This happens between the roots of the function, $I_1(s/\lambda_a) = 0$ and when s/λ_a is an integer.

large, i.e., $N \to \infty$, then I_1'/N reduces to

$$I_1 = \frac{\lambda_a}{8s}\left(2\left\lfloor \frac{s}{\lambda_a}\right\rfloor + 1\right)\left[1 + \frac{\lambda_a^2}{3s^2}\left\lfloor \frac{s}{\lambda_a}\right\rfloor\left(\left\lfloor \frac{s}{\lambda_a}\right\rfloor + 1\right)\right] - \frac{1}{3},$$

such that $s/\lambda_a \notin \mathbb{Z}$. The explicit steps that are used in this derivation are presented in Appendix A. This expression can be solved for s/λ_a in the integral ranges $\lfloor s/\lambda_a \rfloor$ and $\lceil s/\lambda_a \rceil$; if $\lfloor s/\lambda_a \rfloor = \zeta$, then

$$\frac{(2\zeta+1)}{s/\lambda_a} + \frac{\zeta(\zeta+1)(2\zeta+1)}{3s^3/\lambda_a^3} \leqslant \frac{8}{3}, \quad s/\lambda_a \in (\zeta, \zeta+1),$$
$$8(s/\lambda_a)^3 - 3(2\zeta+1)(s/\lambda_a)^2 - \zeta(\zeta+1)(2\zeta+1) \geqslant 0. \tag{19}$$

The equality for Eq. (19) holds for only one root in the integral range $(\zeta, \zeta+1)$. If that root is s^*, then the range for s that satisfies the required inequality is $s \in [s^*, \zeta\lambda_a) = [s^*, \lceil s/\lambda_a \rceil \lambda_a)$.

In Fig. 3, we plot the quantity I_1 as a function of the distance (normalized to the wavelength of the emitted light) between the individual atoms in the array s/λ_a. In the regions where $I_1(s/\lambda_a)$ is negative, the condition of Eq. (17) is satisfied, and the decay is subradiance only. This happens between the roots of the function, $I_1(s/\lambda_a) = 0$, and when s/λ_a is an integer.

Uniform 2D array of atoms. In the case of a 2D ordered array of atoms at equal spacing of length s in both directions with the atomic dipole vector $\vec{\epsilon}_a$ aligned perpendicular to the plane of the array, like in the 1D case, the condition of Eq. (17) gives

$$\left\{I_2'(s/\lambda_a) = \sum_{u,v,u\neq v} \mathcal{J}[2\pi(s/\lambda_a)d_{uv}]\right\} \leqslant 0, \tag{20}$$

where $d_{uv} = [(u_x - v_x)^2 + (u_y - v_y)^2]^{1/2}$ and $u_x, u_y, v_x, v_y \in \{1, \ldots, \sqrt{N}\}$. We can rewrite the sum I_2' as

$$I_2' = \sum_{u_x,u_y}\left[\sum_{p,q\in A(u_x,u_y)} \mathcal{J}[2\pi(s/\lambda_a)\sqrt{p^2+q^2}] + \sum_{p,q\in B(u_x,u_y)} \mathcal{J}[2\pi(s/\lambda_a)\sqrt{p^2+q^2}]\right.$$
$$\left. + \sum_{p,q\in C(u_x,u_y)} \mathcal{J}[2\pi(s/\lambda_a)\sqrt{p^2+q^2}] + \sum_{p,q\in D(u_x,u_y)} \mathcal{J}[2\pi(s/\lambda_a)\sqrt{p^2+q^2}]\right]. \tag{21}$$

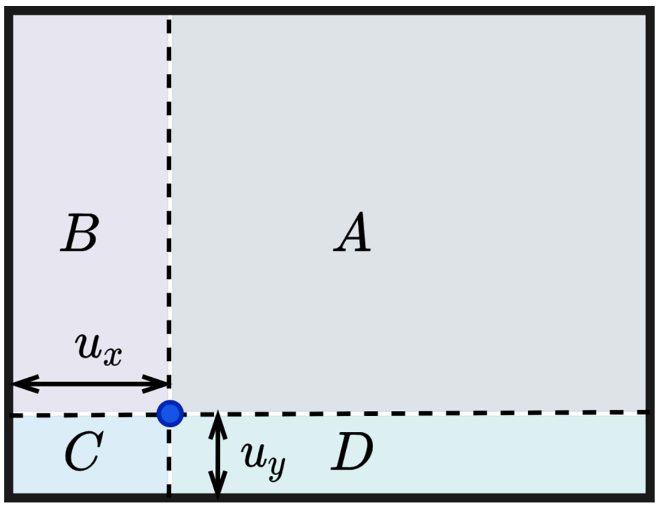

FIG. 4. Four different regions that are seen by the atom at a position of (u_x, u_y). The calculation of the quantity $I_2'(s/\lambda_a)$ requires a summation over all the atoms in each of these regions, A, B, C, and D. In the limit of a large number of atoms, $N \to \infty$, regions A, B, C, and D become identical (see text for details).

We now note that in the limit of a large number of atoms, $N \to \infty$, the four regions A, B, C, and D in Fig. 4 become identical for all atoms, resulting in the simple infinite sum

$$\lim_{N\to\infty} \frac{I_2'}{4N} = I_2 = \sum_{m=1}^{\infty}\sum_{n=0}^{\infty} \mathcal{J}(2\pi s_\lambda\sqrt{m^2+n^2}) \leqslant 0. \tag{22}$$

As before, this can be reduced to

$$I_2 = \frac{\lambda_a^3}{8\pi s^3}\sum_{u,v\in\mathbb{Z}} \frac{(u^2+v^2)\beta_+[\sqrt{u^2+v^2}/(s/\lambda_a)]}{\sqrt{(s/\lambda_a)^2 - (u^2+v^2)}} - \frac{1}{6},$$

such that $s/\lambda_a \notin \{\sqrt{u^2+v^2} : (u,v) \in \mathbb{Z}^2\}$. The proof of this result can be found in Appendix B. The sum in I_2 is only over all the integers u and v strictly inside the circle $u^2 + v^2 = (s/\lambda_a)^2$, as denoted by the β_+ step function above,

$$\beta_+(x) = \begin{cases} 1, & 0 \leqslant x < 1, \\ 0, & \text{otherwise.} \end{cases} \tag{23}$$

A plot of I_2 vs s/λ_a is shown in Fig. 5. As we can see, the points of discontinuity are exactly the points from the set $\{\sqrt{u^2+v^2} : (u,v) \in \mathbb{Z}^2\}$, and the trend of the range of values of I_2 goes with the length of the interval in s/λ_a where it is defined. Moreover, for $s/\lambda_a < 1$, the value of $I_2 = -1/6$ over the whole range, implying that an arranged uniformly excited 2D array of atoms experiences subradiance-only decay if the spacing $s < \lambda_a$.

Two-dimensional disordered ensemble of atoms. For this case, we confine the atoms in a 2D plane of dimensions $L \times L$ such that the minimum separation between the atoms at any

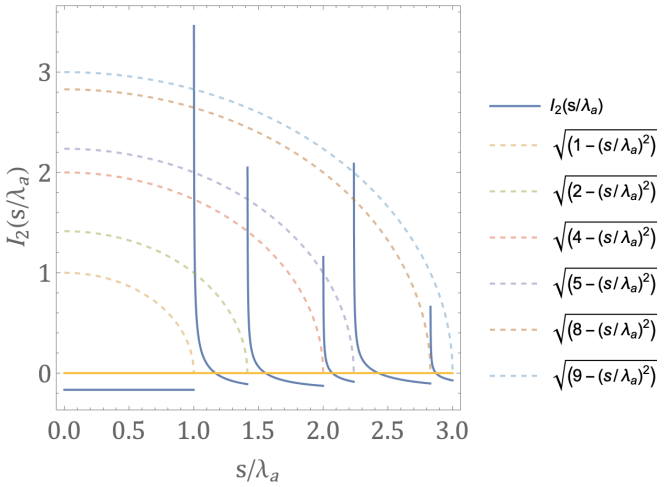

FIG. 5. Plot of I_2 as a function of s/λ_a. In the regions where $I_2(s/\lambda_a)$ is negative, the decay is subradiance only. The plot also illustrates the positions of its singularities. The function is defined everywhere except the points in the set $\{\sqrt{u^2+v^2} : (u, v) \in \mathbb{Z}^2\}$ marked by dashed radial lines.

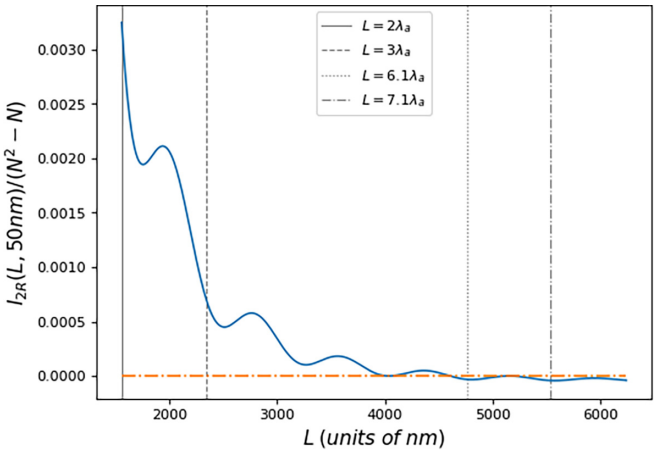

FIG. 6. Graph of $I_{2R}/(N^2 - N)$ versus L for $d = 50$ nm and $\lambda_a = 780$ nm for a 2D disordered ensemble of atoms. The dependence of I_{2R} on L changes sign after roughly $5\lambda_a$ and remains negative for the rest of the domain. This suggests that the system will experience early-time superradiance decay until a domain size of $\sim 5\lambda_a$. For larger domain sizes, decay will be subradiance only. We pick four specific points, which are indicated by vertical lines, and verify the collective decay behavior through direct numerical simulation in Fig. 7.

instant of time is at least d. The position of an atom is uniformly distributed over the whole plane; i.e., the components of the position vector $\vec{R}_u = (X_u, Y_u)$ are uniformly chosen in the open set $(0, L)$, $X_u, Y_u \sim \text{Uniform}(0, L)$. A schematic of this spatial arrangement is shown in Fig. 1(b).

For concreteness, instead of working in normalized units, in this section and the next, we consider the D_2 line transition in rubidium atoms at a transition wavelength of $\lambda_a = 780$ nm. Assuming that the atomic dipole vector is normal to the plane of the atoms, the condition of Eq. (17) then becomes

$$I_{2R} = \mathbb{E}_{\{X_{uv}, Y_{uv}\}}\left[\sum_{u,v,u\neq v} \mathcal{J}\left(k_a\sqrt{X_{uv}^2 + Y_{uv}^2}\right)\right] \leqslant 0. \tag{24}$$

Since we have $R_{uv} = (X_{uv}^2 + Y_{uv}^2)^{1/2}$, we can transform the distribution of the atomic positions from (X_{uv}, Y_{uv}) to $R_{uv} = (X_{uv}^2 + Y_{uv}^2)^{1/2}$. Equation (24) I_{2R} can be rewritten as

$$\begin{aligned} I_{2R}(L, d, N) &= \underbrace{\int_{-\infty}^{\infty}}_{(N^2-N)} \sum_{u,v,u\neq v} \mathcal{J}(k_a R_{uv}) \prod_{u,v,u\neq v} p_r(R_{uv}) dR_{uv} \qquad (25) \\ &= \sum_{u,v,u\neq v} \int_d^{\sqrt{2}L} \mathcal{J}(k_a r) p_r(r) dr \\ &\quad \times \prod_{u,v,R_{uv}\neq r} \int_d^{\sqrt{2}L} p_R(R_{uv}) dR_{uv} \qquad (26) \\ &= (N^2 - N) \int_d^{\sqrt{2}L} \mathcal{J}(k_a r) p_r(r|d) dr. \qquad (27) \end{aligned}$$

The details of the transformations from (X_u, Y_u) to R_{uv} and the expression for $p_r(r|d)$ are outlined in Appendix C. In Fig. 6, we compute the integral of Eq. (27) numerically and graph $I_{2R}/(N^2 - N)$ vs L. In this calculation, we fix the minimum separation between the atoms to $d = 50$ nm. As seen in Fig. 6, the function remains positive up to a domain size of roughly $5\lambda_a$ and then becomes negative. This suggests that the system will experience early-time superradiance decay until a domain size of $\sim 5\lambda_a$. For larger domain sizes, there will be subradiance-only decay.

To verify the analytical predictions of Fig. 6, we also simulate the system numerically. Here, we randomly pick the positions of the individual atoms from the uniform distribution and calculate the evolution of wave function by numerically solving Schrodinger's equation. In Fig. 7, we plot the numerically calculated expectation value of Φ over 1000 iterations for 25 atoms for the four specific cases of $L = 2\lambda_a, 3\lambda_a, 6.1\lambda_a$, and $7.1\lambda_a$. In Fig. 8 we follow the same procedure for 100 iterations and 250 atoms. These four selected cases are shown by the vertical lines in Fig. 6. In agreement with the predictions of Fig. 6, $L = 2\lambda_a$ and $L = 3\lambda_a$ display early-time superradiance, while $L = 6.1\lambda_a$ and $L = 7.1\lambda_a$ show subradiance-only decay. In Figs. 7 and 8, the curves that go below the zero line (dashed line) display early-time superradiance, while the curves that always remain above the zero-line are subradiance-only decay.

Three-dimensional disordered ensemble of atoms. For the case of a 3D ensemble of atoms, we confine the atoms in a cube of length L with minimum separation d. In the analytical and numerical results that we discuss below, this minimum separation is chosen to be $d/\lambda_a = 0.06$. We checked that all the results that we discuss below are not sensitive to the exact value of this minimum separation between the atoms. The atomic dipole vector $\vec{\epsilon}_a$ is assumed to be pointing towards the z axis. A schematic of this arrangement is provided in Fig. 1(c). In this case, again under the assumption of uniform excitation of the atomic ensemble, the condition of Eq. (17)

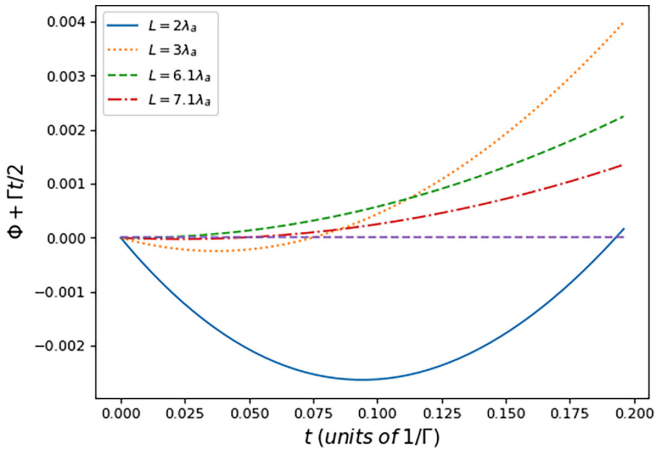

FIG. 7. The numerically calculated expectation value of Φ over 1000 iterations for 25 atoms for four specific cases: $L = 2\lambda_a, 3\lambda_a, 6.1\lambda_a$, and $7.1\lambda_a$. These four selected cases are shown by the vertical lines in Fig. 6. Since the uncorrelated decay rate of $\ln \|\phi(t)\|$ is $-\Gamma/2$, it becomes the dashed zero line in this plot. All the other decay processes can be understood as deviations from this line, as illustrated in Fig. 2. In agreement with the predictions of Fig. 6, $L = 2\lambda_a$ and $L = 3\lambda_a$ display early-time superradiance, while $L = 6.1\lambda_a$ and $L = 7.1\lambda_a$ show subradiance-only decay.

using Eqs. (4)–(7) becomes

$$I_{3R} = \mathbb{E}_{\{X_{uv},Y_{uv},Z_{uv}\}}\Bigg[\sum_{u,v,u\neq v} \mathcal{J}\big(k_a\sqrt{X_{uv}^2+Y_{uv}^2+Z_{uv}^2}\big) + \frac{Z_{uv}^2}{X_{uv}^2+Y_{uv}^2+Z_{uv}^2}\mathcal{K}\big(k_a\sqrt{X_{uv}^2+Y_{uv}^2+Z_{uv}^2}\big)\Bigg] \leqslant 0. \tag{28}$$

We will discuss the initial condition that is different from the uniform excitation below. Like before, instead of working with the Cartesian coordinates of the individual atoms, we define $R_{uv} = (X_{uv}^2 + Y_{uv}^2 + Z_{uv}^2)^{1/2}$ and $C_{uv} = Z_{uv}/R_{uv}$. Therefore, we transform the random variables X_{uv}, Y_{uv}m and Z_{uv} into R_{uv} and C_{uv}. The derivation of the transformation and resulting probability distribution $p_{rc}(r, c|d)$ is carried out in Appendix D. The expression for I_{3R} in the transformed basis is

$$I_{3R}(L, d, N) = (N^2 - N) \times \int_d^{\sqrt{3}L}\int_{-1}^{1}[\mathcal{J}(k_a r) + c^2\mathcal{K}(k_a r)] \times p_{rc}(r, c|d)dcdr. \tag{29}$$

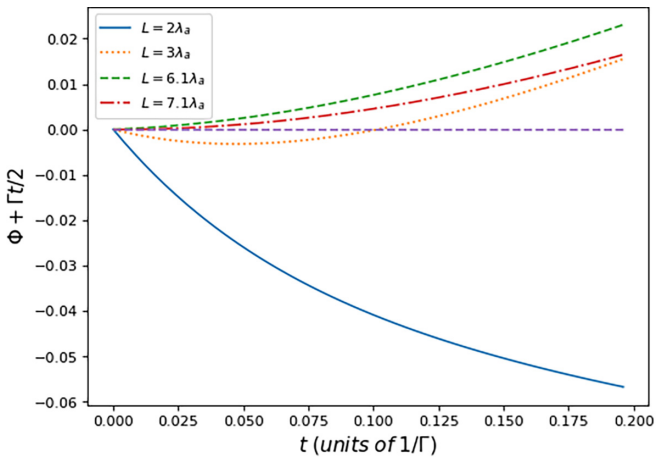

FIG. 8. Similar to Fig. 7, the numerically calculated expectation value of Φ over 100 iterations for 250 atoms for the same four cases of $L = 2\lambda_a, 3\lambda_a, 6.1\lambda_a$, and $7.1\lambda_a$. The results are again in agreement with the predictions of Fig. 6.

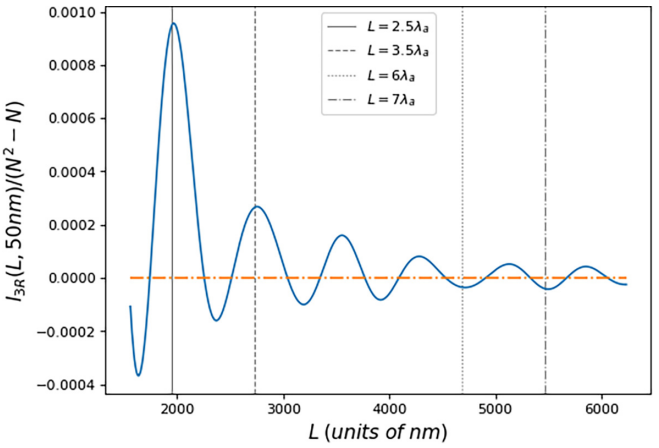

FIG. 9. Graph of $I_{3R}/(N^2 - N)$ versus L for $d = 50$ nm and $\lambda_a = 780$ nm for a 3D disordered ensemble of atoms. The function shows oscillatory behavior, and in the regions where $I_{3R}/(N^2 - N) < 0$, the decay is subradiance only. We pick four specific points, which are indicated by vertical lines, and verify the collective decay behavior through direct numerical simulation in Figs. 10 and 11.

Numerically performing the integral for $d = 50$ nm like before, we obtain the plot in Fig. 9. The integral oscillates as a function of the domain size, showing specific regions where the decay will exhibit superradiance or will be subradiance only.

Like above, we confirm the predictions of Fig. 9 by numerically integrating the Schrodinger's equation and calculating the evolution of the wave function. Figures 10 and 11 show the results for four specific domain sizes, which are indicated by the vertical lines in Fig. 9. The expectation value of Φ is again calculated over 1000 iterations with 25 atoms. In agreement with the analytical result of Fig. 9, two curves display superradiance, while the other two show subradiance-only decay.

We note that for a 3D ensemble, the assumption of uniform excitation is, in general, not a good assumption. For example, if the initial excitation is performed using a laser beam, the phase of the propagating laser will be imprinted on the initial excitation amplitude. We next discuss subradiance-only decay in a 3D ensemble when the initial excitation is performed using a laser beam. Instead of the uniformly excited initial state $\phi_u(0) = 1/\sqrt{N}$, we now consider an initial state with a phase imprinted due to the laser propagating along the x direction. As a result, the new initial state for the 3D

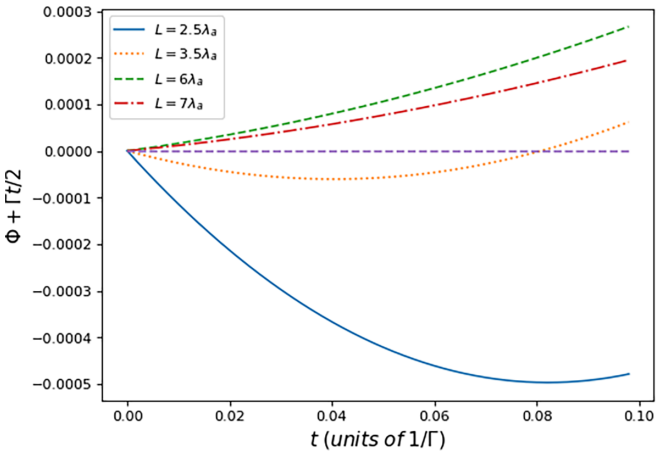

FIG. 10. The numerically calculated expectation value of Φ over 1000 iterations for 25 atoms for four specific cases that are shown by the vertical lines in Fig. 9. In agreement with the predictions of Fig. 8, $L = 2.5\lambda_a$ and $L = 3.5\lambda_a$ display early-time superradiance, while $L = 6\lambda_a$ and $L = 7\lambda_a$ show subradiance-only decay.

ensemble is

$$\phi_u(0) = e^{ik_{\text{laser}}\, x_u}\frac{1}{\sqrt{N}}. \tag{30}$$

We consider the simplest case where the frequency of the laser equals the frequency of the atomic excitation and therefore take $k_{\text{laser}} \approx k_a$. This initial relative phase causes phase mismatch in Eq. (14), which then results in

$$\Phi'(0) = \text{Im}\sum_{u,v} e^{-ik_a x_{uv}} H_{uv}/N. \tag{31}$$

As a result of this modified equation, the condition for the absence of early-time superradiance in Eq. (17) transforms to

$$\frac{2}{\Gamma}\text{Im}\sum_{u,v,u\neq v} e^{-ik_a x_{uv}} H_{uv} \geqslant 0. \tag{32}$$

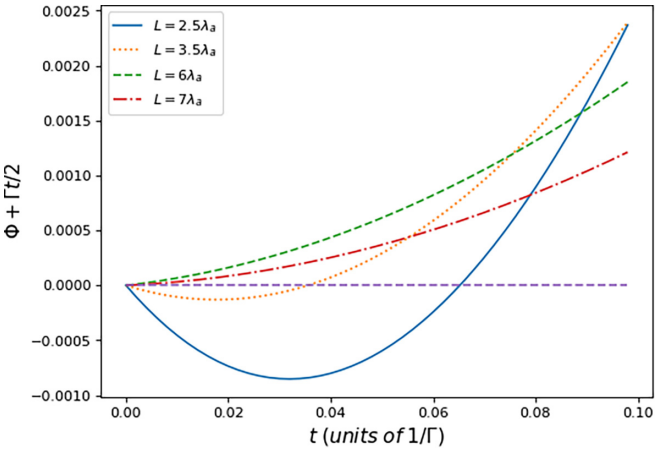

FIG. 11. Similar to Fig. 10, the numerically calculated expectation value of Φ over 100 iterations for 250 atoms for the same four cases that are shown by the vertical lines in Fig. 9. The results are again in agreement with the predictions of Fig. 9.

Equation (32) is more difficult to evaluate analytically due to the presence of the phase terms $e^{-ik_a x_{uv}}$. To simplify what follows, instead of a 3D ensemble with a cube-shaped volume, we consider a spherical atomic ensemble with a Gaussian probability distribution of radius R_0. With this setup the expression for I_{3R}, which is the negative of the left-hand side of the new condition in Eq. (32), becomes

$$I_{3R} = \frac{3}{2}\mathbb{E}_{\{R_{uv},\theta_{uv},\phi_{uv}\}}\sum_{u,v,u\neq v}\cos(k_a R_{uv}\cos\phi_{uv}\sin\theta_{uv}) \times [\mathcal{J}(k_a R_{uv}) + \cos^2\theta_{uv}\mathcal{K}(k_a R_{uv})]. \tag{33}$$

For each coordinate the Gaussian distribution is given by

$$p_g(X) = \frac{1}{\sqrt{\pi R_0^2}} e^{-X^2/R_0^2}. \tag{34}$$

Under the coordinate transformation $D_x = X_1 - X_2$ and $I = X_2$, the new distribution is

$$p_{12}(D_x) = \int_{-\infty}^{\infty}\frac{p_g(D_x + I)p_g(I)}{J(D_x, I)}\, dI, \tag{35}$$

where $J(D_x, I)$ is the Jacobian of transformation at the intersection point $X_1 = D_x + I, X_2 = I$. Using the result from Eq. (C2) in Appendix C, we have $J = 1$, which then results in

$$p_{12}(D_x) = \frac{1}{\pi R_0^2} e^{-D_x^2/R_0^2}\int_{-\infty}^{\infty} e^{-2(I^2 + D_x I)/R_0^2} dI = \frac{1}{\sqrt{2\pi R_0^2}} e^{-D_x^2/(2R_0^2)}. \tag{36}$$

We then multiply the distribution for all coordinates together to obtain

$$p_{12}(D) = \frac{1}{\left(2\pi R_0^2\right)^{3/2}} e^{-D^2/(2R_0^2)}. \tag{37}$$

As a result, the expression for I_{3R} now transforms to

$$I_{3R} = \frac{3}{2\left(2\pi R_0^2\right)^{3/2}}(N^2 - N) \times \int_0^{\infty}\int_0^{\pi}\int_0^{2\pi}\cos(k_a r\cos\phi\sin\theta)[\mathcal{J}(k_a r) + \cos^2\theta\ \mathcal{K}(k_a r)] e^{-r^2/(2R_0^2)} r^2\sin\theta\ dr\ d\theta\ d\phi. \tag{38}$$

The above integral can be performed analytically, which then gives the following final expression:

$$I_{3R} = \frac{3(N^2 - N)}{2} e^{-k_a^2 R_0^2} \times \frac{\left[\left(R_0^4 k_a^4 + 1\right)\sinh\left(R_0^2 k_a^2\right) - R_0^2 k_a^2\cosh\left(R_0^2 k_a^2\right)\right]}{R_0^6 k_a^6}. \tag{39}$$

There is a correction term due to the minimum allowable distance between the atoms d. This correction term is at the level of 10^{-5} for $d/\lambda_a \lesssim 0.06$. Since I_{3R} is positive for all

values of R_0, there will, on average, always be superradiance [following Eq. (32)]. This result suggests that subradiance-only decay does not happen in a disordered ensemble with a spherical volume when the initial state is excited with a laser beam.

IV. CONCLUSIONS AND DISCUSSION

In conclusion, we discussed analytically and numerically that, under certain parameters, subradiance does not necessarily need to be accompanied by early-time superradiance. We focused on the single-atom excited subspace (i.e., weak-excitation regime) and showed that the ensemble can immediately start to decay with a rate which is slower than the independent decay rate. We identified the parameter regimes in one, two, and three dimensions where such subradiance-only decay can happen.

We note that the robustness of the subradiance-only decay can be deduced from the variation of the functions I_1, I_2, I_{2R}, and I_{3R} to their argument. These functions are plotted in Figs. 3, 5, 6, and 9, and subradiance-only decay occurs in the regions where the functions are negative. These functions vary reasonably smoothly as a function of the parameters of the system, for example, s/λ_a in ordered arrays (where the quantity s is the spacing between the atoms) and L in disordered ensembles (which is the overall size of the ensemble). As a result, the regions where these functions are negative happen over a sizable domain, which indicates the robustness of the effect to the variations in the parameters of the system. The exceptions to this happen near the singularities of the functions.

To give a specific example, in Fig. 3, we plot I_1 as a function of s/λ_a for a 1D ordered array. The function I_1 has singularities at integer values of s/λ_a, $s/\lambda_a = 1, 2, 3, \ldots$. Near these integer values, the subradiance-only decay is not robust and depends sensitively on the array spacing. However, in other regions, the function is smooth, and the effect is robust. For example, for $s/\lambda_a = 0.7$ the decay is subradiance only, and $\pm 20\%$ of the fluctuations in the array spacing will still display subradiance-only decay.

We note that in our approach we used a simplified two-level approach (i.e., a scalar model), and we ignored the vectorial nature and the polarization properties of light. While it is known that the simplified scalar model captures many aspects of collective decay [49], there can also be significant differences between the predictions of the scalar and vectorial models in certain scenarios. For example, recent work on the Anderson localization of light showed that the vectorial nature of light destroys Anderson localization [50]. One future direction is to extend our results to multilevel atomic systems interacting with light while taking into account the vectorial nature and the polarization properties of the light.

One exciting future direction is to pursue experimental observations of these predictions. By extending recent observations of subradiance in dilute ultracold clouds with low optical depth, it should be possible to verify many of the results presented in Figs. 7, 8, 10, and 11. Another future direction is to extend these results to the strong-excitation regime, where the evolution is not confined to the single-excited subspace of the Hilbert space.

ACKNOWLEDGMENTS

We thank D. Gold and U. Saglam for many helpful discussions. This work was supported by National Science Foundation (NSF) Grant No. 2016136 for the QLCI center Hybrid Quantum Architectures and Networks (HQAN) and also by the University of Wisconsin–Madison through the Vilas Associates Award.

APPENDIX A: ANALYTIC EXPRESSION FOR A LINEAR ARRAY OF ATOMS

To find the sum of $\mathcal{J}(x)$ we need to find the sum of appropriate expressions involving spherical Bessel functions. For brevity we will use the shorthand s_λ for s/λ_a. Note that as $N \to \infty$, we need to evaluate only two infinite sums because

$$I_1 = \lim_{N\to\infty} \sum_{m=1}^{N} (N-m)\mathcal{J}(2\pi s_\lambda m) \leqslant 0 \tag{A1}$$

$$= \lim_{N\to\infty} \sum_{m=1}^{N} \mathcal{J}(2\pi s_\lambda m) - \lim_{N\to\infty} \sum_{m=1}^{N} \frac{m}{N} \mathcal{J}(2\pi s_\lambda m) \leqslant 0 \tag{A2}$$

$$= \sum_{m=1}^{\infty} \mathcal{J}(2\pi s_\lambda m) \leqslant 0 \Rightarrow \sum_{m=1}^{\infty} \left(j_0(2\pi s_\lambda m) - \frac{j_1(2\pi s_\lambda m)}{2\pi s_\lambda m} \right) \leqslant 0, \tag{A3}$$

provided that the sum $\sum_m m\mathcal{J}(2\pi s_\lambda m)$ is finite. Since

$$\sum_{m=1}^{\infty} m\mathcal{J}(2\pi s_\lambda m) = \sum_{m=1}^{\infty} \frac{\sin(2\pi s_\lambda m)}{2\pi s_\lambda} + \frac{1}{4\pi^2 s_\lambda^2} \sum_{m=1}^{\infty} \frac{\cos(2\pi s_\lambda m)}{m} - \frac{1}{8\pi^3 s_\lambda^3} \sum_{m=1}^{\infty} \frac{\sin(2\pi s_\lambda m)}{m^2}, \tag{A4}$$

the first sum is finite for all values of s_λ; the second sum converges to $-\ln[2\sin(\pi s_\lambda)]$, which is finite only when $s_\lambda \notin \mathbb{Z}$, and the third sum is also finite for all s_λ except at zero, where it has a double pole. Therefore, the sum of I_1 can be evaluated by summing over only $j_0(2\pi s_\lambda m)$ and $j_1(2\pi s_\lambda m)/(2\pi s_\lambda m)$ provided that $s_\lambda \notin \mathbb{Z}$.

To find the infinite sum we use the Poisson summation formula, which states that for a Schwarz function, say, $f : \mathbb{R} \to \mathbb{C}$ and $L \in \mathbb{R}^+$,

$$\sum_{n=-\infty}^{\infty} f(nL) = \frac{1}{L} \sum_{k=-\infty}^{\infty} \tilde{f}\left(\frac{2\pi k}{L}\right), \tag{A5}$$

where $\tilde{f}$ is the Fourier transform of f,

$$\tilde{f}(k) = \int_{-\infty}^{\infty} e^{-ikz} f(z) dz, \quad f(z) = \frac{1}{2\pi} \int_{-\infty}^{\infty} e^{ikz} \tilde{f}(k) dk. \tag{A6}$$

Taking $L = 2\pi s_\lambda$, (A5) becomes

$$\sum_{n=-\infty}^{\infty} f(2\pi s_\lambda n) = \frac{1}{2\pi s_\lambda} \sum_{k=-\infty}^{\infty} \tilde{f}(k/s_\lambda); \tag{A7}$$

for the purpose here, we investigate the case when $f \equiv j_\ell$. Using the integral representation of the spherical Bessel

functions,

$$j_\ell(z) = \frac{1}{2i^\ell}\int_{-1}^{1} e^{izt}P_\ell(t)dt, \tag{A8}$$

we obtain

$$\tilde{j}_\ell(k) = \int_{-\infty}^{\infty} e^{-ikz}j_\ell(z)dz = \frac{1}{2i^\ell}\int_{-1}^{1}\int_{-\infty}^{\infty} e^{i(t-k)z}P_\ell(t)dzdt = \frac{\pi}{i^\ell}\int_{-1}^{1}\delta(t-k)P_\ell(t)dt = \frac{\pi}{i^\ell}\beta(k)P_\ell(k), \tag{A9}$$

and subsequently,

$$\sum_{n=-\infty}^{\infty} j_\ell(2\pi s_\lambda n) = \frac{1}{2\pi s_\lambda}\sum_{k=-\infty}^{\infty}\tilde{j}_\ell(k/s_\lambda) = \frac{1}{2\pi s_\lambda}\frac{\pi}{i^\ell}\sum_{k=-\infty}^{\infty}\beta\left(\frac{k}{s_\lambda}\right)P_\ell\left(\frac{k}{s_\lambda}\right) = \frac{1}{2i^\ell s_\lambda}\sum_{-s_\lambda<k<s_\lambda} P_\ell(k/s_\lambda). \tag{A10}$$

We can now use (A10), the identity,

$$j'_\ell(z) = j_{\ell-1}(z) - \frac{\ell+1}{z}j_\ell(z), \tag{A11}$$

and the fact that the Fourier transform of f' is $ik\tilde{f}$ to find the sum of $j_\ell(z)/z$. First, we find the sum for $j'_\ell(2\pi s_\lambda m)$,

$$\sum_{n=-\infty}^{\infty} j'_\ell(2\pi s_\lambda n) = \frac{1}{2\pi s_\lambda}\sum_{k=-\infty}^{\infty} i\frac{k}{s_\lambda}\tilde{j}_\ell(k/s_\lambda) = \frac{1}{2i^{\ell-1}s_\lambda^2}\sum_{-s_\lambda<k<s_\lambda} kP_\ell(k/s_\lambda); \tag{A12}$$

hence,

$$\frac{1}{(\ell+1)}\left(\sum_{n=-\infty}^{\infty} j_{\ell-1}(2\pi s_\lambda n) - \sum_{n=-\infty}^{\infty} j'_\ell(2\pi s_\lambda n)\right) = \sum_{n=-\infty}^{\infty}\frac{j_\ell(2\pi s_\lambda n)}{2\pi s_\lambda n} \tag{A13}$$

or

$$\frac{1}{2}\left(\sum_{n=-\infty}^{\infty} j_0(2\pi s_\lambda n) - \sum_{n=-\infty}^{\infty} j'_1(2\pi s_\lambda n)\right) = \sum_{n=-\infty}^{\infty}\frac{j_1(2\pi s_\lambda n)}{2\pi s_\lambda n},$$

$$\frac{1}{4}\left(\frac{1}{s_\lambda}\sum_{-s_\lambda<k<s_\lambda} P_0(k/s_\lambda) - \frac{1}{s_\lambda^2}\sum_{-s_\lambda<k<s_\lambda} kP_1(k/s_\lambda)\right) = \sum_{n=-\infty}^{\infty}\frac{j_1(2\pi s_\lambda n)}{2\pi s_\lambda n}. \tag{A14}$$

Finally, substituting $\ell = 0$ in (A10) and (A14), we find

$$\sum_{n=-\infty}^{\infty}\mathcal{J}(2\pi s_\lambda n) = \frac{1}{2s_\lambda}\sum_{-s_\lambda<k<s_\lambda} P_0(k/s_\lambda) - \frac{1}{4s_\lambda}\sum_{-s_\lambda<k<s_\lambda} P_0(k/s_\lambda) + \frac{1}{4s_\lambda^2}\sum_{-s_\lambda<k<s_\lambda} kP_1(k/s_\lambda). \tag{A15}$$

Using the fact that $\mathcal{J}(x)$ is an even function and that $\mathcal{J}(0) = 2/3$, we get

$$\sum_{n=1}^{\infty}\mathcal{J}(2\pi s_\lambda n) = \frac{1}{8s_\lambda^2}\sum_{-s_\lambda<k<s_\lambda}[s_\lambda P_0(k/s_\lambda) + kP_1(k/s_\lambda)] - \frac{1}{3} = \frac{1}{8}\left(\frac{1}{s_\lambda}\sum_{k=-\lfloor s_\lambda\rfloor}^{\lfloor s_\lambda\rfloor} 1 + \frac{1}{s_\lambda^3}\sum_{k=-\lfloor s_\lambda\rfloor}^{\lfloor s_\lambda\rfloor} k^2\right) - \frac{1}{3} \tag{A16}$$

$$= \frac{1}{8s_\lambda}(2\lfloor s_\lambda\rfloor+1) + \frac{1}{24s_{\lambda^3}}\lfloor s_\lambda\rfloor(\lfloor s_\lambda\rfloor+1)(2\lfloor s_\lambda\rfloor+1) - \frac{1}{3} = \frac{(2\lfloor s_\lambda\rfloor+1)}{8s_\lambda}\left(1 + \frac{\lfloor s_\lambda\rfloor(\lfloor s_\lambda\rfloor+1)}{3s_{\lambda^2}}\right) - \frac{1}{3}, \tag{A17}$$

such that $s_\lambda \notin \mathbb{Z}$.

APPENDIX B: ANALYTIC EXPRESSION FOR THE TWO-DIMENSIONAL ARRAY OF ATOMS

Before the derivation we introduce two notational functions, β and β_+, as follows:

$$\beta(x) = \begin{cases} 1, & |x| < 1, \\ 0, & |x| > 1, \end{cases} \qquad \beta_+(x) = \begin{cases} 1, & 0 \leqslant x < 1, \\ 0, & \text{otherwise.} \end{cases} \tag{B1}$$

To find the sum $I'_2/4N$ in the limit $N \to \infty$ we apply the higher-dimensional version of the Poisson summation formula with Hankel transforms to reduce the infinite sum to a tractable finite sum. The Poisson summation formula as stated in Appendix A

also has the following 2D form:

$$\sum_{\vec{n}\in\mathbb{Z}^2} f(\vec{n}L) = \frac{1}{L^2}\sum_{\vec{k}\in\mathbb{Z}^2} \tilde{f}\left(\frac{2\pi\vec{k}}{L}\right), \tag{B2}$$

with $L = 2\pi s_\lambda$, $\vec{n} = (m, n)$, $\|\vec{n}\| = \sqrt{n^2+m^2} = r$, $\vec{k} = (u, v)$, and $\|\vec{k}\| = \sqrt{u^2+v^2} = \rho$. To apply this formula to the sum in (41) we must first find its two-dimensional Fourier transform. We must note that the function $\mathcal{J}(2\pi s_\lambda\sqrt{x^2+y^2}) = \mathcal{J}(2\pi s_\lambda r)$ is circularly symmetric, implying that its Fourier transform can be found via its Hankel transform. The Hankel transform $\bar{f}(\rho)$ of a circularly symmetric function $f(r)$ is defined as follows:

$$\bar{f}(\rho) = \int_0^\infty f(r)J_0(r\rho)rdr, \quad J_0(w) = \frac{1}{2\pi}\int_{-\pi}^{\pi} e^{iw\cos(\theta-\varphi)}d\theta, \tag{B3}$$

where J_0 denotes the Bessel function of order zero. It can easily be shown that the Fourier transform and the Hankel transform are related by the substitution of $x = r\cos\theta$, $y = r\sin\theta$, $u = \rho\cos\varphi$, and $v = \rho\sin\varphi$ in the following equation:

$$\tilde{f}(\vec{k}) = \tilde{f}(u, v) = \int_{-\infty}^{\infty}\int_{-\infty}^{\infty} e^{-i(ux+vy)}f(x, y)dxdy = \int_0^\infty f(r)2\pi J_0(r\rho)rdr = 2\pi\bar{f}(\rho) = 2\pi\bar{f}(\sqrt{u^2+v^2}). \tag{B4}$$

From the definition of the spherical Bessel functions in terms of the Bessel functions of half-integer order, we have

$$\frac{j_n}{r^n} = \sqrt{\frac{\pi}{2}}\frac{J_{n+\frac{1}{2}}}{r^{n+\frac{1}{2}}}. \tag{B5}$$

The Hankel transform of $J_\ell(r)/r^\ell$ is known to be $(1-\rho^2)^{\ell-1}\beta_+(\rho)/[2^{\ell-1}\Gamma(\ell)]$; therefore, the Hankel transform of $j_\ell(r)/r^\ell$ is

$$\frac{j_\ell(r)}{r^\ell} \leftrightarrow_H \sqrt{\frac{\pi}{2}}\frac{(1-\rho^2)^{\ell-\frac{1}{2}}}{2^{\ell-\frac{1}{2}}\Gamma\left(\ell+\frac{1}{2}\right)}\beta_+(\rho) = \sqrt{\frac{\pi}{2}}\frac{2^{2\ell}\ell!(1-\rho^2)^{\ell-\frac{1}{2}}}{2^{\ell-\frac{1}{2}}(2\ell)!\sqrt{\pi}}\beta_+(\rho) = \frac{2^\ell\ell!}{(2\ell)!}(1-\rho^2)^{\ell-\frac{1}{2}}\beta_+(\rho). \tag{B6}$$

Hence, the 2D Fourier transform of $j_\ell(r)/r^\ell$ is

$$\frac{j_\ell(r)}{r^\ell} \leftrightarrow_F 2\pi\frac{2^\ell\ell!}{(2\ell)!}(1-\rho^2)^{\ell-\frac{1}{2}}\beta_+(\rho). \tag{B7}$$

Finally, substituting $\ell = 0$ and 1, respectively,

$$j_0(r) \leftrightarrow_F 2\pi\frac{\beta_+(\rho)}{\sqrt{1-\rho^2}}, \quad \frac{j_1(r)}{r} \leftrightarrow_F 2\pi\beta_+(\rho)\sqrt{1-\rho^2}. \tag{B8}$$

Applying the Poisson summation formula to each of them and then subtracting, we obtain

$$\sum_{m,n} j_0(2\pi s_\lambda\sqrt{m^2+n^2}) = \frac{1}{(2\pi s_\lambda)^2}\sum_{u,v} 2\pi\frac{\beta_+(\rho/s_\lambda)}{\sqrt{1-(\rho/s_\lambda)^2}}, \tag{B9}$$

$$\sum_{m,n}\frac{j_1(2\pi s_\lambda\sqrt{m^2+n^2})}{2\pi s_\lambda\sqrt{m^2+n^2}} = \frac{1}{(2\pi s_\lambda)^2}\sum_{u,v} 2\pi\beta_+(\rho/s_\lambda)\sqrt{1-(\rho/s_\lambda)^2}, \tag{B10}$$

$$\sum_{m,n}\mathcal{J}(2\pi s_\lambda\sqrt{m^2+n^2}) = \frac{1}{2\pi s_\lambda^2}\sum_{u,v}\beta_+(\rho/s_\lambda)\left(\frac{1}{\sqrt{1-(\rho/s_\lambda)^2}} - \sqrt{1-(\rho/s_\lambda)^2}\right) \tag{B11}$$

$$\Rightarrow 4\sum_{m=1}^{\infty}\sum_{n=1}^{\infty}\mathcal{J}(2\pi s_\lambda\sqrt{m^2+n^2}) + 4\sum_{m=1}^{\infty}\mathcal{J}(2\pi s_\lambda m) + \mathcal{J}(0) = \frac{1}{2\pi s_\lambda^4}\sum_{u,v}\frac{\rho^2\beta_+(\rho/s_\lambda)}{\sqrt{1-(\rho/s_\lambda)^2}}, \tag{B12}$$

and so

$$\lim_{N\to\infty}\frac{I_2'}{4N} = \sum_{m=1}^{\infty}\sum_{n=0}^{\infty}\mathcal{J}(2\pi s_\lambda\sqrt{m^2+n^2}) = \frac{1}{8\pi s_\lambda^4}\sum_{u,v}\frac{\rho^2\beta_+(\rho/s_\lambda)}{\sqrt{1-(\rho/s_\lambda)^2}} - \frac{1}{6} = \frac{1}{8\pi s_\lambda^3}\sum_{u,v\in\mathbb{Z}}\frac{(u^2+v^2)\beta_+(\sqrt{u^2+v^2}/s_\lambda)}{\sqrt{s_\lambda^2-(u^2+v^2)}} - \frac{1}{6}, \tag{B13}$$

such that $s_\lambda \notin \{\sqrt{u^2+v^2} : (u, v) \in \mathbb{Z}\times\mathbb{Z}\}$.

APPENDIX C: DERIVATION OF THE PROBABILITY DISTRIBUTION FOR R_{uv}

To find the distribution of R_{uv} we first derive the probability distribution of X_{uv} and Y_{uv} from that of $X_u, Y_u \sim \text{Uniform}(0, L)$ and then apply the transformation of random variables from X_{uv} and Y_{uv} to $R_{uv} = \sqrt{X_{uv}^2+Y_{uv}^2}$.

Let $X_1, X_2 \sim \text{Uniform}(0, L)$, such that

$$p_U(X_i) = \frac{\beta_+(X_i/L)}{L}; \tag{C1}$$

then let the following transformation of variables be applied: $D = X_1 - X_2$ and $B = X_2$. The intersection points of the lines $D(X_1, X_2)$ and $B(X_1, X_2)$ are $X_1 = D + B$ and $X_2 = B$, and the Jacobian of transformation at the point of intersection is

$$J(X_1, X_2) = \begin{vmatrix} \frac{\partial D}{\partial X_1} & \frac{\partial D}{\partial X_2} \\ \frac{\partial B}{\partial X_1} & \frac{\partial B}{\partial X_2} \end{vmatrix} = \begin{vmatrix} 1 & -1 \\ 0 & 1 \end{vmatrix} = 1. \tag{C2}$$

The corresponding transformation to the probability distribution will be

$$p_\Lambda(D) = \int_0^\infty p_U(D + B, B)/|J(D + B, B)|dB = \int_0^L \frac{\beta_+((D + B)/L)}{L^2} dB. \tag{C3}$$

Since $0 < X_1, X_2 < L$ implies that $-L < X_1 - X_2 < L$ or $-L < D < L$, and from $\beta_+[(D + B)/L]$, $B \in (-A, L - A) \cap (0, L)$. Therefore, when $-L < D < 0$, $-A < B < L$, and when $0 < A < L$, $0 < B < L - A$. Thus,

$$p_\Lambda(A) = \begin{cases} \int_{-A}^{L} \frac{1}{L^2} dB = \frac{L+A}{L^2}, & -L < A < 0, \\ \int_0^{L-A} \frac{1}{L^2} dB = \frac{L-A}{L^2}, & 0 < A < L, \end{cases} = \frac{L - |A|}{L^2} \beta(A/L). \tag{C4}$$

We call this distribution $\Lambda(-L, L)$; hence, we have proved that $X_{uv}, Y_{uv} \sim \Lambda(-L, L)$.

Next, we similarly transform, say, $X, Y \sim \Lambda(-L, L)$ to $R = \sqrt{X^2 + Y^2}$, $T = Y$. The intersection of curves R and T is at $X = \pm\sqrt{R^2 - T^2}$, $Y = T$. The Jacobian of transformation is as follows:

$$J(X, Y) = \begin{vmatrix} \frac{\partial R}{\partial X} & \frac{\partial R}{\partial Y} \\ \frac{\partial T}{\partial X} & \frac{\partial T}{\partial Y} \end{vmatrix} = \begin{vmatrix} \frac{X}{R} & \frac{Y}{R} \\ 0 & 1 \end{vmatrix} = \frac{X}{R}. \tag{C5}$$

The values at the intersection points are $J_1 = J(\sqrt{R^2 - T^2}, T) = \sqrt{R^2 - T^2}/R$ and $J_2 = J(-\sqrt{R^2 - T^2}, T) = -\sqrt{R^2 - T^2}/R$. Hence, the probability distribution for R is

$$p_r(R) = \int_{-\infty}^{\infty} \left(\frac{p_\Lambda(\sqrt{R^2 - T^2}, T)}{|J_1|} + \frac{p_\Lambda(-\sqrt{R^2 - T^2}, T)}{|J_2|} \right) dT = 2R \int_{-\infty}^{\infty} \frac{p_\Lambda(\sqrt{R^2 - T^2}, T)}{\sqrt{R^2 - T^2}} dT \tag{C6}$$

$$= \frac{4R}{L^4} \int_0^L \frac{(L - \sqrt{R^2 - T^2})(L - T)}{\sqrt{R^2 - T^2}} \beta\left(\frac{\sqrt{R^2 - T^2}}{L} \right) dT. \tag{C7}$$

Solving the last integral, we obtain the following function:

$$p_r(R) = \begin{cases} 0 & R < 0, \\ \frac{2R(L^2\pi - 4LR + R^2)}{L^4} & 0 \leqslant R \leqslant L, \\ \frac{4R}{L^4}\left[\frac{1}{L^2} \sin^{-1}\left(2\frac{L^2}{R^2} - 1\right) - L^2 - \frac{R^2}{2} + 2L\sqrt{R^2 - L^2} \right] & L < R \leqslant \sqrt{2}L, \\ 0 & R > \sqrt{2}L. \end{cases} \tag{C8}$$

Last, because the minimum separation distance is restricted to d, we renormalize the probability distribution $p_r(R)$ by the factor

$$\mathcal{N}(d) = \int_d^{\sqrt{2}L} p_r(r)dr = 1 - \int_0^d p_r(r)dr = 1 - \int_0^{2\pi} \int_0^d p_\Lambda(r\cos\theta) p_\Lambda(r\sin\theta) r dr d\theta, \tag{C9}$$

giving us

$$p_r(r|d) = p_r(r)/\mathcal{N}(d) = \frac{6L^4}{6L^4 + 16d^3L - 6L^2d^2\pi - 3d^4}$$

$$\times \begin{cases} 0 & r < d, \\ \frac{2r(L^2\pi - 4Lr + r^2)}{L^4} & d \leqslant r \leqslant L, \\ \frac{4r}{L^4}\left[\frac{1}{L^2} \sin^{-1}\left(2\frac{L^2}{r^2} - 1\right) - L^2 - \frac{r^2}{2} + 2L\sqrt{r^2 - L^2} \right] & L < r \leqslant \sqrt{2}L, \\ 0 & r > \sqrt{2}L. \end{cases} \tag{C10}$$

APPENDIX D: DERIVATION OF THE PROBABILITY DISTRIBUTION FOR R_{uv} and C_{uv}

Based on the same principles as in Appendix C, we define transformation of variables from X_{uv}, Y_{uv}, and Z_{uv} to $R_{uv} = \sqrt{X_{uv}^2 + Y_{uv}^2 + Z_{uv}^2}$ and $C_{uv} = Z_{uv}/R_{uv}$. Therefore, let $X, Y, Z \sim \Lambda(-L, L)$, and we define three transformed variables: $R = \sqrt{X^2 + Y^2 + Z^2}$, $C = Z/R$, and $W = X$. The intersection points of the surfaces R, C, and W are $X = W$, $Y = \pm\sqrt{R^2(1 - C^2) - W^2}$, and $Z = RC$. The Jacobian of the transformation

$$J(X, Y, Z) = \begin{vmatrix} \frac{\partial R}{\partial X} & \frac{\partial R}{\partial Y} & \frac{\partial R}{\partial Z} \\ \frac{\partial C}{\partial X} & \frac{\partial C}{\partial Y} & \frac{\partial C}{\partial Z} \\ \frac{\partial W}{\partial X} & \frac{\partial W}{\partial Y} & \frac{\partial W}{\partial Z} \end{vmatrix} = \begin{vmatrix} \frac{X}{R} & \frac{Y}{R} & \frac{Z}{R} \\ -\frac{ZX}{R^3} & -\frac{ZY}{R^3} & \frac{X^2+Y^2}{R^3} \\ 1 & 0 & 0 \end{vmatrix} = \frac{Y}{R^4}(X^2 + Y^2 + Z^2) = \frac{Y}{R^2}. \tag{D1}$$

At the intersection points the Jacobian values are $J_1 = J(W, \sqrt{R^2(1 - C^2) - W^2}, RC) = \sqrt{R^2(1 - C^2) - W^2}/R^2$ and $J_2 = J(W, -\sqrt{R^2(1 - C^2) - W^2}, RC) = -\sqrt{R^2(1 - C^2) - W^2}/R^2$. The final distribution is then

$$p_{rc}(R, C) = \int_{-\infty}^{\infty} \left(\frac{p_d(W, \sqrt{R^2(1 - C^2) - W^2}, RC)}{|J_1|} + \frac{p_d(W, -\sqrt{R^2(1 - C^2) - W^2}, RC)}{|J_2|} \right) dW \tag{D2}$$

$$= \frac{4R^2(L - |RC|)}{L^6} \beta\left(\frac{RC}{L}\right) \int_0^L \frac{(L - W)[L - \sqrt{R^2(1 - C^2) - W^2}]}{\sqrt{R^2(1 - C^2) - W^2}} \beta\left(\frac{\sqrt{R^2(1 - C^2) - W^2}}{L}\right) dW. \tag{D3}$$

After the correct intersection regions are isolated, the above integral reduces to the following probability distribution function:

$$p_{rc}(R, C) = \frac{4R^2(L - |RC|)}{L^6}$$

$$\times \begin{cases} -2\sqrt{1 - C^2}LR + \frac{1}{2}(1 - C^2)R^2 + \frac{\pi L^2}{2}, & 0 \leqslant R \leqslant L, |C| < 1, \\ 2L\sqrt{(1 - C^2)R^2 - L^2} + L^2 \sin^{-1}\left(\frac{2L^2}{(1-C^2)R^2} - 1\right) - \frac{(1-C^2)R^2}{2} - L^2, & L < R \leqslant \sqrt{2}L, |C| < \sqrt{1 - \frac{L^2}{R^2}}, \\ -2\sqrt{1 - C^2}LR + \frac{1}{2}(1 - C^2)R^2 + \frac{\pi L^2}{2}, & L < R \leqslant \sqrt{2}L, \sqrt{1 - \frac{L^2}{R^2}} \leqslant |C| < \frac{1}{\sqrt{2}}, \\ 2L\sqrt{(1 - C^2)R^2 - L^2} + L^2 \sin^{-1}\left(\frac{2L^2}{(1-C^2)R^2} - 1\right) - \frac{(1-C^2)R^2}{2} - L^2, & \sqrt{2}L < R \leqslant \sqrt{3}L, \sqrt{1 - \frac{2L^2}{R^2}} \leqslant |C| < \frac{1}{\sqrt{3}}, \\ 0, & \text{otherwise.} \end{cases} \tag{D4}$$

Renormalizing as before, we obtain

$$p_{rc}(r, c|d) = \frac{120r^2(L - |rc|)}{30L^6 + 5d^6 - 48d^5L + 45\pi d^4L^2 - 40\pi d^3L^3} \tag{D5}$$

$$\times \begin{cases} -2\sqrt{1 - c^2}Lr + \frac{1}{2}(1 - c^2)r^2 + \frac{\pi L^2}{2}, & d \leqslant r \leqslant L, |c| < 1, \\ 2L\sqrt{(1 - c^2)r^2 - L^2} + L^2 \sin^{-1}\left(\frac{2L^2}{(1-c^2)r^2} - 1\right) - \frac{(1-c^2)r^2}{2} - L^2, & L < r \leqslant \sqrt{2}L, |c| < \sqrt{1 - \frac{L^2}{r^2}}, \\ -2\sqrt{1 - c^2}Lr + \frac{1}{2}(1 - c^2)r^2 + \frac{\pi L^2}{2}, & L < r \leqslant \sqrt{2}L, \sqrt{1 - \frac{L^2}{r^2}} \leqslant |c| < \frac{1}{\sqrt{2}}, \\ 2L\sqrt{(1 - c^2)r^2 - L^2} + L^2 \sin^{-1}\left(\frac{2L^2}{(1-c^2)r^2} - 1\right) - \frac{(1-c^2)r^2}{2} - L^2, & \sqrt{2}L < r \leqslant \sqrt{3}L, \sqrt{1 - \frac{2L^2}{r^2}} \leqslant |c| < \frac{1}{\sqrt{3}}, \\ 0, & \text{otherwise.} \end{cases} \tag{D6}$$

[1] R. H. Dicke, Coherence in spontaneous radiation processes, Phys. Rev. **93**, 99 (1954).

[2] M. Gross and S. Haroche, Superradiance: An essay on the theory of collective spontaneous emission, Phys. Rep. **93**, 301 (1982).

[3] M. O. Scully and A. A. Svdzinsky, The super of superradiance, Science **325**, 1510 (2009).

[4] H. Ma, O. Rubies-Bigorda, and S. F. Yelin, Superradiance and subradiance in a gas of two-level atoms, arXiv:2205.15255.

[5] F. Robicheaux and D. A. Suresh, Beyond lowest order mean-field theory for light interacting with atom arrays, Phys. Rev. A **104**, 023702 (2021).

[6] R. J. Bettles, S. A. Gardiner, and C. S. Adams, Cooperative eigenmodes and scattering in one-dimensional atomic arrays, Phys. Rev. A **94**, 043844 (2016).

[7] S. D. Jenkins and J. Ruostekoski, Controlled manipulation of light by cooperative response of atoms in an optical lattice, Phys. Rev. A **86**, 031602(R) (2012).

[8] H. Zoubi and H. Ritsch, Metastability and directional emission characteristics of excitons in 1D optical lattices, Europhys. Lett. **90**, 23001 (2010).

[9] C. E. Máximo, R. Bachelard, F. E. A. dos Santos, and C. J. Villas-Boas, Cooperative spontaneous emission via a renormalization approach: Classical versus semiclassical effects, Phys. Rev. A **101**, 023829 (2020).

[10] D. F. Kornovan, A. S. Sheremet, and M. I. Petrov, Collective polaritonic modes in an array of two-level quantum emitters coupled to an optical nanofiber, Phys. Rev. B **94**, 245416 (2016).

[11] D. Bhatti, R. Schneider, S. Oppel, and J. von Zanthier, Directional Dicke subradiance with nonclassical and classical light sources, Phys. Rev. Lett. **120**, 113603 (2018).

[12] R. Wiegner, J. von Zanthier, and G. S. Agarwal, Quantum-interference-initiated superradiant and subradiant emission from entangled atoms, Phys. Rev. A **84**, 023805 (2011).

[13] M. Reitz, C. Sommer, and C. Genes, Cooperative quantum phenomena in light-matter platforms, PRX Quantum **3**, 010201 (2022).

[14] N. Skribanowitz, I. P. Herman, J. C. MacGillivray, and M. S. Feld, Observation of Dicke superradiance in optically pumped HF gas, Phys. Rev. Lett. **30**, 309 (1973).

[15] R. Friedberg, S. R. Hartmann, and J. T. Manassah, Frequency shifts in emission and absorption by resonant systems of two-level atoms, Phys. Rep. **7**, 101 (1973).

[16] J. Rui, D. Wei, A. Rubio-Abadal, S. Hollerith, J. Zeiher, D. M. Stamper-Kurn, C. Gross, and I. Bloch, A subradiant optical mirror formed by a single structured atomic layer, Nature (London) **583**, 369 (2020).

[17] J. Kim, D. Yang, S. Oh, and K. An, Coherent single-atom superradiance, Science **359**, 662 (2018).

[18] J. A. Greenberg and D. J. Gauthier, Steady-state, cavityless, multimode superradiance in a cold vapor, Phys. Rev. A **86**, 013823 (2012).

[19] Y. Yoshikawa, Y. Torii, and T. Kuga, Superradiant light scattering from thermal atomic vapors, Phys. Rev. Lett. **94**, 083602 (2005).

[20] R. G. DeVoe and R. G. Brewer, Observation of superradiant and subradiant spontaneous emission of two trapped ions, Phys. Rev. Lett. **76**, 2049 (1996).

[21] B. H. McGuyer, M. McDonald, G. Z. Iwata, M. G. Tarallo, W. Skomorowski, R. Moszynski, and T. Zelevinsky, Precise study of asymptotic physics with subradiant ultracold molecules, Nat. Phys. **11**, 32 (2015).

[22] C. Bradac, M. T. Johnsson, M. v. Breugel, B. Q. Baragiola, R. Martin, M. L. Juan, G. K. Brennen, and T. Volz, Room-temperature spontaneous superradiance from single diamond nanocrystals, Nat. Commun. **8**, 1205 (2017).

[23] A. Angerer, K. Streltsov, T. Astner, S. Putz, H. Sumiya, S. Onoda, J. Isoya, W. J. Munro, K. Nemoto, J. Schmiedmayer, and J. Majer, Superradiant emission from color centers in diamond, Nat. Phys. **14**, 1168 (2018).

[24] Z. Wang, H. Li, W. Feng, X. Song, C. Song, W. Liu, Q. Guo, X. Zhang, H. Dong, D. Zheng, H. Wang, and D.-W. Wang, Controllable switching between superradiant and subradiant states in a 10-qubit superconducting circuit, Phys. Rev. Lett. **124**, 013601 (2020).

[25] W. Guerin, M. O. Araujo, and R. Kaiser, Subradiance in a large cloud of cold atoms, Phys. Rev. Lett. **116**, 083601 (2016).

[26] P. Weiss, M. O. Araújo, R. Kaiser and W. Guerin, Subradiance and radiation trapping in cold atoms, New J. Phys. **20**, 063024 (2018).

[27] T. Bienaime, N. Piovella, and R. Kaiser, Controlled Dicke subradiance from a large cloud of two-level systems, Phys. Rev. Lett. **108**, 123602 (2012).

[28] A. Cipris, N. A. Moreira, T. S. do Espirito Santo, P. Weiss, C. J. Villas-Boas, R. Kaiser, W. Guerin, and R. Bachelard, Subradiance with saturated atoms: Population enhancement of the long-lived states, Phys. Rev. Lett. **126**, 103604 (2021).

[29] P. Weiss, A. Cipris, M. O. Araujo, R. Kaiser, and W. Guerin, Robustness of Dicke subradiance against thermal decoherence, Phys. Rev. A **100**, 033833 (2019).

[30] G. Ferioli, A. Glicenstein, L. Henriet, I. Ferrier-Barbut, and A. Browaeys, Storage and release of subradiant excitations in a dense atomic cloud, Phys. Rev. X **11**, 021031 (2021).

[31] A. Glicenstein, G. Ferioli, A. Browaeys, and I Ferrier-Barbut, From superradiance to subradiance: Exploring the many-body Dicke ladder, Opt. Lett. **47**, 1541 (2022).

[32] G. Ferioli, A. Glicenstein, F. Robicheaux, R. T. Sutherland, A. Browaeys, and I. Ferrier-Barbut, Laser-Driven superradiant ensembles of two-level atoms near Dicke regime, Phys. Rev. Lett. **127**, 243602 (2021).

[33] D. Das, B. Lemberger, and D. D. Yavuz, Subradiance and superradiance-to-subradiance transition in dilute atomic clouds, Phys. Rev. A **102**, 043708 (2020).

[34] D. C. Gold, P. Huft, C. Young, A. Safari, T. G. Walker, M. Saffman, and D. D. Yavuz, Spatial coherence of light in collective spontaneous emission, PRX Quantum **3**, 010338 (2022).

[35] E. Shahmoon, D. S. Wild, M. D. Lukin, and S. F. Yelin, Cooperative resonances in light scattering from two-dimensional atomic arrays, Phys. Rev. Lett. **118**, 113601 (2017).

[36] O. Rubies-Bigorda, S. Ostermann, and S. F. Yelin, Dynamic population of multiexcitation subradiant states in incoherently excited atomic arrays, Phys. Rev. A **107**, L051701 (2023).

[37] R. T. Sutherland and F. Robicheaux, Coherent forward broadening in cold atom clouds, Phys. Rev. A **93**, 023407 (2016).

[38] D. A. Suresh and F. Robicheaux, Photon-induced atom recoil in collectively interacting planar arrays, Phys. Rev. A **103**, 043722 (2021).

[39] F. Robicheaux, Theoretical study of early-time superradiance for atom clouds and arrays, Phys. Rev. A **104**, 063706 (2021).

[40] H. Zoubi and H. Ritsch, Lifetime and emission characteristics of collective electronic excitations in two-dimensional optical lattices, Phys. Rev. A **83**, 063831 (2011).

[41] K. E. Ballantine and J. Ruostekoski, Quantum single photon control, storage, and entanglement generation with planar atomic arrays, PRX Quantum **2**, 040362 (2021).

[42] E. Sierra, S. J. Masson, and A. Ansejo-Garcia, Dicke superradiance in ordered lattices: Dimensionality matters, Phys. Rev. Res. **4**, 023207 (2022).

[43] J. Xu, S. Chang, Y. Tang, S. Zhu, and G. S. Agarwal, Hyperradiance accompanied by nonclassicality, Phys. Rev. A **96**, 013839 (2017).

[44] M. Pleinert, J. von Zanthier, and G. S. Agarwal, Hyperradiance from collective behavior of coherently driven atoms, Optica **4**, 779 (2017).

[45] A. Asenjo-Garcia, M. Moreno-Cardoner, A. Albrecht, H. J. Kimble, and D. E. Chang, Exponential improvement in photon storage fidelities using subradiance and selective radiance in atomic arrays, Phys. Rev. X **7**, 031024 (2017).

[46] G. Ferioli, A. Glicenstein, I. Ferrier-Barbut, and A. Browaeys, A non-equilibrium superradiant phase transition in free space, Nat. Phys. **19**, 1345 (2023).

[47] Z. Yan, J. Ho, Y.-H. Lu, S. J. Masson, A. Asenjo-Garcia, and D. M. Stamper-Kurn, Superradiant and subradiant cavity scattering by atom arrays, Phys. Rev. Lett. **131**, 253603 (2023).

[48] B. Lemberger and D. D. Yavuz, Effect of correlated decay on fault-tolerant quantum computation, Phys. Rev. A **96**, 062337 (2017).

[49] L. Bellando, A. Gero, E. Akkermans, and R. Kaiser, Roles of cooperative effects and disorder in photon localization: The case of a vector radiation field, Eur. Phys. J. B **94**, 49 (2021).

[50] S. E. Skipetrov and I. M. Sokolov, Absence of Anderson localization of light in a random ensemble of point scatterers, Phys. Rev. Lett. **112**, 023905 (2014).